

Precomputed 1D-CNNs for Atrial Fibrillation Detection on Tiny Smart Sensor Systems

Lukas Einhaus, Natalie Maman, Julian Hoever, Andreas Erbslöh, Gregor Schiele
Intelligent Embedded Systems Lab, University of Duisburg-Essen,
Faculty of Computer Science, Duisburg, Germany
{first-name}.{last-name}@uni-due.de

Abstract—1D-CNNs play a crucial role for time-series analysis on tiny smart sensor systems, e.g. for biosignal analysis, predictive maintenance, or structural health monitoring. LUT-based precomputation has emerged as an interesting optimization technique to implement such neural networks on FPGAs. The core idea is to precompute all possible outputs of a neural network layer and store them directly in the lookup tables of the FPGAs. This enables highly resource-efficient networks with ultra-low latency but suffers from poor scalability. Previous work has explored using depthwise-separable convolutions to improve scalability. In this paper, we generalize this approach to consider additional forms of grouped convolutions. Based on this, we propose a novel type of convolutional block and an algorithm to guide the choice of hyper parameters for this block. We evaluate our approach on a medical time-series dataset for predicting atrial fibrillation using the MIT-BIH database (ECG recordings). The resulting hardware accelerators are small enough to be deployed on an AMD Spartan-7 S15. They achieve a F1-score of up to 95.6% while only requiring 2,844 LUTs and no DSPs or BRAM.

Index Terms—1D convolutional neural network, precomputed, embedded deep learning, low-latency, resource-efficiency

I. INTRODUCTION

Smart sensor systems combine sensing technology with on-device machine learning to process sensor data locally. This enhances privacy, reaction time, and offline availability.

One dimensional convolutional neural networks (1D-CNNs) have been shown to be a well suited machine learning approach for this, usable in a diverse set of application fields, such as structural health monitoring [1], predictive maintenance [2], [3] and various medical applications [4]–[7]. While transformer architectures gained a lot of traction in recent years, 1D-CNNs can still provide a more suitable trade-off between performance and resource requirements. Especially in very small sensor systems, transformer architectures can quickly exceed time or energy constraints [8]. To speed up the computation of 1D-CNNs, our work uses small-scale Field Programmable Gate Arrays (FPGAs) like the Spartan 7 S15 to implement efficient hardware accelerators [9]. FPGAs contain thousands of lookup tables (LUTs) that can implement small Boolean functions, e.g., a function with 4 or 6 inputs (each 1 bit) and an 1 bit output, depending on the selected FPGA. Together, these can emulate arbitrary hardware circuits, ranging, e.g., from adders and multipliers to whole CPUs.

Our work goes one step further, making use of the fact that LUTs can reduce arbitrarily complex functions to a value

lookup of constant time complexity. Using this, we *precompute* neural network components, such as a filter in a convolutional layer or a neuron in a linear layer and represent them as truth tables that can be stored in the FPGA’s LUTs. This is especially useful for ultra-low latency applications. The main challenge with this approach is to limit the exponential growth of the precomputed truth tables, which depends on the number of input bits to the implemented function. We will refer to this number as fan in. For a function with I inputs with a bitwidth of b , the resulting truth table is made up of $2^{b \cdot I}$ entries. Therefore, it is crucial to minimize fan in for each network component as much as possible. Previous work has resorted to random sparsity [10], [11] or lossy function representations for dense neural networks [12].

For 1D-CNNs, previous work has used depthwise separable convolutions to reduce the fan in for precomputed convolutions [13]. This works well for small kernels but does not scale for more complex architectures. Therefore, it is necessary to explore more possibilities for replacing conventional convolutions. In this paper, we propose to use the more general concept of *grouped convolutions* [14] instead of depthwise separable convolutions. This can lead to extreme cost reductions while achieving similar accuracy. More specifically, we make the following contributions:

- We propose a configurable grouped convolutional block to replace conventional dense convolutions. Such blocks can be used to split a convolution into a sequence of two convolutions that can be precomputed and represented with a small number of LUTs on FPGAs.
- We introduce a score to rate the above-mentioned configurations wrt. network performance vs. resource consumption to help selecting favourable configurations without having to try out all possible configurations.
- We provide an open source tool to generate synthesizable hardware designs based on our approach and evaluate their performance on real hardware.

The remainder of our paper is structured as follows. After a discussion of related work in Section II, we present our approach for precomputing 1D-CNNs on FPGAs in Section III. We evaluate our approach in Section IV using the MIT-BIH dataset [15] and conclude the paper in Section V.

II. RELATED WORK

In the following section, we discuss related work for LUT-based precomputation approaches in deep neural networks.

A number of approaches tries to reduce the fan in of network components. LogicNets [10] shows an approach for networks composed of linear layers. The authors reduce area consumption by initializing neurons with random sparsity. PolyLUT [11] presents a generalization of LogicNets, replacing all computations between the input and output of a neuron by a single LUT. They consider not only linear transformations of the input data, but also polynomial ones, thus taking advantage of the fact that a LUT can represent arbitrary Boolean functions. The resulting model has a higher flexibility to fit the data, potentially needing fewer layers to represent the same function. The increase in LUT size is thus compensated by the layer savings which at the same time improves latency. Similarly, NeuralUT [16] represents whole sub-networks by a single LUT. These sub-networks are composed of multiple fully-connected layers that use floating-point precision inside sub-nets, while keeping the cost low by using quantization and sparsity between sub-nets.

Another set of approaches focusses on compressing truth tables of precomputed functions. Khatei et al. [17] decompose truth tables and combine the results during runtime using simple primitives. Others additionally record which input values can actually be observed during training and inject *don't care* for everything else to increase the potential for compression [12], [18], [19].

Petersen et al. make networks composed of primitive binary logic gates (LGNs) differentiable, leading to ultra-sparse low complexity neural networks [20] and apply that approach to 2D-CNNs maintaining 80.17% accuracy on CIFAR-10, while decreasing inference times by a factor of 160 [21].

Weightless neural networks (WNNs) [22] use *RAM-Nodes* (essentially truth tables) as building blocks for neural networks also during training. Consequently, they are typically not trained with gradient descent. Bacellar et al. extend the approach for differentiable logic gates from Petersen and apply it to WNNs to obtain differentiable WNNs (DWNs), improving accuracy compared to NeuralUT, while reducing resource consumption roughly by a factor of up to 200. Nag et al. present a vision transformer (ViT) architecture incorporating DWNs [23]. While this improves accuracy from 57.5% to 95.5% on CIFAR-10 compared to Bacellar et al., it drastically increases the number of LUTs from 46k to 587k.

None of these approaches focuses on 1D-CNNs for ultra low-power FPGAs with only a few thousand LUTs.

III. OUR APPROACH

We propose an automated way to derive LUT-based hardware accelerators for resource-constrained smart sensor systems from existing off-the-shelf 1D-CNNs defined in PyTorch. To achieve this, our approach has to decrease the fan in of the network's components drastically and explore the trade-off between resource consumption and network performance. The obtained network architectures are trained as

usual and automatically translated to a hardware description language (HDL). The resulting accelerators do not need any block RAM (BRAM) or DSP slices for multiplications.

Our approach can be broken down into five steps: (i) binarize activations, (ii) use our Split Convolutional Block, that is based on grouped convolutions, to replace dense convolutions, (iii) filter the number of potential candidates for said replacements heuristically, (iv) identify precomputable structures and compute their corresponding truth tables, (v) convert the result into HDL.

A. Binary Activations for Precomputable Blocks

Replacing full-resolution with binary activations is not only a straight-forward way to reduce the fan in, it also allows for fine-grained control of the fan in by varying the input channels of convolutions. We binarize activations by using

$$\text{bin}(x) = \begin{cases} 1 & \text{if } x \geq 0 \\ -1 & \text{else} \end{cases} \quad (1)$$

in the forward pass and replace the gradient with the straight-through-estimator (STE) $\frac{\partial}{\partial x} \text{bin} = 1$ for the backward pass [24]. Weights will only be represented implicitly on hardware, and are kept at full resolution.

We use the binary activations in the network architecture to identify blocks that are precomputable, i.e., that can be represented via LUTs. We can include more components between two binary activations to increase the capacity of precomputed blocks without additional cost, as long as this does not increase the fan in of the corresponding block.

B. LUT Cost

Before describing our Split Convolutional Block, we first introduce an analytical cost model to estimate the required physical LUT count. This model will also be used by our toolchain, later. Without it, we would need to synthesize costs from HDL, which takes a lot of time.

As this analytical model does not include any heuristic logic optimizations, it represents a worst case estimation. The actual resource consumption of hardware resulting from synthesis will typically be much lower. Similarly to the pattern shown

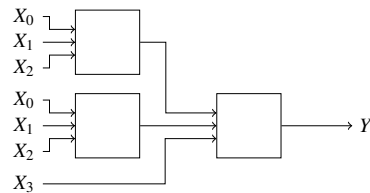


Fig. 1: Exemplary composition of higher fan in ($n = 4$) truth table composed of three 3:1-LUTs

in Figure 1, one can construct n :1-truth tables using 3:1-LUTs in hardware. We denote the LUT count for a n bit truth table with C_n . Using AMD FPGAs like Spartan 7 with 6:1-LUTs, there we distinguish between three cases: $n \leq 6$, $n = 7 + 2l$ (for odd cases) and $n = 8 + 2l$ (for even cases) with $l \in \mathbb{N}_0$.

For $n \leq 6$ we can directly implement the truth table with a single LUT. For $n = 7 + 2l$, we obtain

$$C_n = 2 \cdot C_{n-1} + 1. \quad (2)$$

For $n = 8 + 2l$, we can build the truth tables from four instances of the LUT tree for $n - 2$ and combine the four results with an additional LUT leading to

$$C_n = 4 \cdot C_{n-2} + 1 = 2 \cdot (C_{n-1} - 1) + 1. \quad (3)$$

Thus, we can estimate the cost of composing a n -to-1 truth table from LUTs using the following recursive relation:

$$C_n = \begin{cases} 1 & \text{if } n \leq 6 \\ 2 \cdot C_{n-1} - (-1)^n & \text{else} \end{cases} \quad (4)$$

From that, we derive the closed form expression for the LUT cost for implementing a X -to- Y truth table (required from logical function) using 6:1-LUTs by:

$$C(X, Y) = \frac{Y}{3} \cdot \left(2^{(X-4)} - (-1)^X \right) \quad (5)$$

We will use this to estimate the cost of convolutional blocks and the resulting neural network.

C. Split Convolutional Blocks

Binary activations alone are usually not enough to obtain hardware accelerators deployable on small FPGAs. Therefore we additionally replace convolutions with our *Split Convolutional Blocks*, which use grouped convolutions to reduce fan in and thus improve scalability.

Grouped convolutions generalize the concept of depthwise convolutions. While a depthwise convolution partitions c channels into g groups with $c = g$ and processes each of them separately, we can choose the number of groups freely for grouped convolutions, as long as

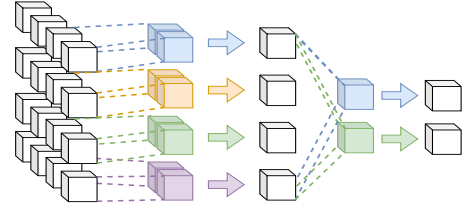
$$\exists s_{\text{in}}, s_{\text{out}} \in \mathbb{N}: s_{\text{in}} \cdot g = c \wedge s_{\text{out}} \cdot g = f, \quad (6)$$

where f is the number of output channels and $s_{\text{in/out}}$ denote the sizes of input and output groups respectively.

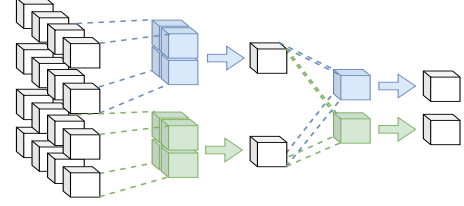
Figure 2 shows in (a) a depthwise separable convolution and in (b) a grouped convolutional block with hyper parameters that allow them to act as a structural replacement for an original dense convolution with four input channels, two output channels and a kernel size of two. This means, that both the number of input channels c and the number of output channels f have to be dividable by g . With k denoting the kernel size, we want to replace a convolution with parameters $F_0 = (c_0, k_0, g_0, f_0)$ by two convolutions with parameters $F_i = (c_i, k_i, g_i, f_i)$, $i \in \{\alpha, \beta\}$ and binary activations. This requires the following condition

$$\begin{aligned} c_0 = c_\alpha = s_{\text{in},\alpha} \cdot g_\alpha \wedge f_\alpha = c_\beta = s_{\text{out},\alpha} \cdot g_\alpha = s_{\text{in},\beta} \cdot g_\beta \\ \wedge f_0 = f_\beta = s_{\text{out},\beta} \cdot g_\beta. \end{aligned} \quad (7)$$

We restrict $(k_\alpha, k_\beta) = (k_0, 1)$, i.e., a Split Convolutional Block ends with a pointwise convolution, similar to depthwise separable convolutions.



(a) Depthwise separable convolution with $(c_\alpha, k_\alpha, g_\alpha, f_\alpha) = (4, 2, 4, 4)$ and $(c_\beta, k_\beta, g_\beta, f_\beta) = (4, 1, 1, 2)$



(b) Grouped convolutional block with $(c_\alpha, k_\alpha, g_\alpha, f_\alpha) = (4, 2, 2, 2)$ and $(c_\beta, k_\beta, g_\beta, f_\beta) = (2, 1, 1, 2)$

Fig. 2: Visualisation of two different convolutional kernels with different colours. We denote the hyper parameter of the convolutional blocks $F = (c, k, g, f)$, with c input channels, a kernel size k , number of groups g and f output channels.

Thus, our proposed Split Convolutional Block (see Figure 3, green area) consists of a convolution with hyper parameters F_α followed by a batch normalization, a binary activation function and another convolution with hyper parameters F_β , to replace the original dense convolution with hyper parameters F_0 , such that F_0, F_α, F_β fulfill the condition from Eq. (7). The resulting LUT cost can be computed as

$$C \left(k_\alpha \cdot \frac{c_0}{g_\alpha}, f_\alpha \right) + C \left(k_\beta \cdot \frac{f_\alpha}{g_\beta}, f_0 \right) \quad (8)$$

This provides fine-grained control of the fan in and hence the LUT cost by varying g .

D. Treatment of Pooling Layers

In XNOR-Net [25], the authors argue that applying a max pooling layer after a binary activation results in significant information loss and thus hurts network performance. They propose a block structure of conv-pool-bnorm-binarize to replace a structure of conv-bnorm-binarize-pool. But for our approach this would combine a convolution and a pooling layer in a single precomputable block. This increases the receptive field of that block and consequently the fan in.

But we can reorder layers for training, such that we use order with higher accuracy during training and our original order with lower resource consumption for precomputation. The left side of Figure 3 shows the change of layer order and the added sign inversion operation after convolution β between training and post training phase. To see why and how we can reorder these layers, let

$$\text{bnorm}_\gamma(x) = \frac{x - \mu}{\sigma^2} \cdot \gamma - \beta \quad (9)$$

be the batchnorm layer, with $\mu \geq 0$, $\sigma > 0$, $\gamma \in \mathbb{R}$ and $\beta \in \mathbb{R}$. Let

$$h(x_1, x_2) = \text{bnorm}_\gamma(\max(x_1, x_2)) \quad (10)$$

With $x_1 > x_2$ we have

$$h(x_1, x_2) = \text{bnorm}_\gamma(x_1) \quad (11)$$

and

$$x_1 > x_2 \Rightarrow \begin{cases} \text{bnorm}_\gamma(x_1) > \text{bnorm}_\gamma(x_2) & \text{if } \gamma > 0 \\ \text{bnorm}_\gamma(x_1) < \text{bnorm}_\gamma(x_2) & \text{else} \end{cases} \quad (12)$$

Thus, for \hat{h} with

$$\hat{h}(x_1, x_2) = \begin{cases} \max(\text{bnorm}_\gamma(x_1), \text{bnorm}_\gamma(x_2)) & \text{if } \gamma > 0 \\ -\max(-\text{bnorm}_\gamma(x_1), -\text{bnorm}_\gamma(x_2)) & \text{else} \end{cases} \quad (13)$$

it follows that

$$h(x_1, x_2) = \hat{h}(x_1, x_2). \quad (14)$$

Because binarization is monotonous, we can reorder layers by multiplying each channel where the batch norm layer has a $\gamma < 0$ with -1 before and after the pooling layer. While the

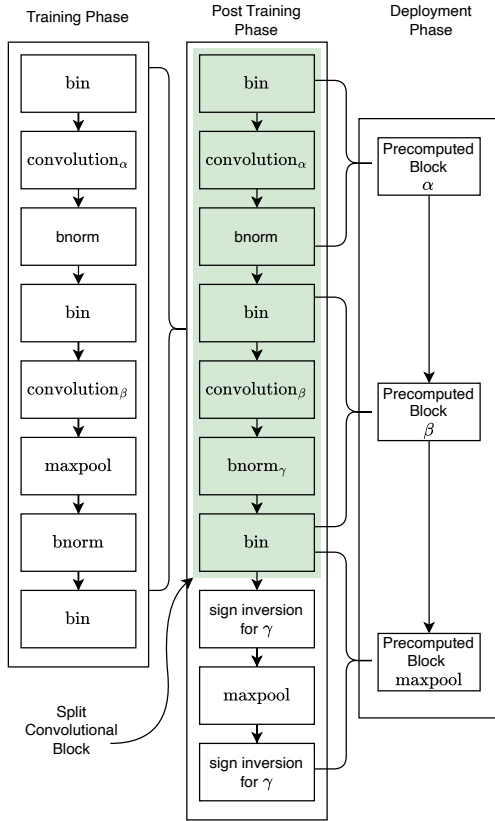


Fig. 3: Different stages of the neural network. The Split Convolutional Block is highlighted green.

order of these layers does not impact the computed result, it does change which weights are updated during the backward pass. Applying pooling first will filter out the features with smaller amplitude.

E. Choosing Split Configurations

Another important design decision is how to choose the split between the two sequential convolutions in our split convolution blocks. These blocks provide a large degree of flexibility. But they also introduce a complex relationship between hyper parameters.

Choosing a split configuration for each layer independently can quickly result in unmanageable large search spaces. Therefore, we introduce a score to rate Split Convolutional Blocks prior to training, that is derived from split configurations. As a first step, we introduce a new metric, we call cross layer connectivity (CLC), to quantify how many of the input channels c_α can influence each of the output channels f_β of a split convolution. We express the fan in of a component as $\phi = k \cdot \frac{c}{g}$ and filter out all split convolutions with

$$\phi_{\max} \geq \max(\phi_\alpha, \phi_\beta) = \max\left(k_\alpha \cdot \frac{c_\alpha}{g_\alpha}, k_\beta \cdot \frac{c_\beta}{g_\beta}\right). \quad (15)$$

We use this constraint in Algorithm 1 to build a set of possible split configurations \mathcal{F} .

Algorithm 1 Finding set of split configurations \mathcal{F} for a given filter $F_0 = (k_0, c_0, f_0, g_0)$ and a maximum fan in ϕ_{\max}

```

1: function FINDFILTERPAIRS( $F_0$ )
2:    $seqs \leftarrow \{(k_0, 1), (1, k_0)\}$   $\triangleright$  Possible kernel size sequences
3:    $\mathcal{F} \leftarrow \emptyset$ 
4:   for all  $k_\alpha, k_\beta \in seqs$  do
5:      $d_\alpha \leftarrow \emptyset$ 
6:     for each  $g_\alpha$  in divisors of  $c_0$  do
7:        $\phi_\alpha \leftarrow (c_0 \div g_\alpha) \cdot k_\alpha$   $\triangleright$  first layer fan in
8:       if  $\phi_\alpha \leq \phi_{\max}$  then
9:          $d_\alpha \leftarrow d_\alpha \cup \{g_\alpha\}$ 
10:      end if
11:     end for
12:     for all  $g_\alpha \in d_\alpha$  do
13:       for all  $g_\beta$  in divisors of  $f_0$  do
14:          $cs \leftarrow \emptyset, c \leftarrow g_\alpha$ 
15:          $\phi_\beta \leftarrow (c \div g_\beta) \cdot k_\beta$   $\triangleright$  second layer fan in
16:         while  $\phi_\beta \leq \phi_{\max}$  do
17:           if  $c \bmod g_\beta = 0$  then
18:              $cs \leftarrow cs \cup c$ 
19:           end if
20:            $c \leftarrow c + g_\alpha$ 
21:            $\phi_\beta \leftarrow (c \div g_\beta) \cdot k_\beta$ 
22:         end while
23:         for all  $c \in cs$  do
24:            $\mathcal{F} \leftarrow \mathcal{F} \cup \{(k_\alpha, c_0, c, g_\alpha),$ 
25:              $(k_\beta, c, f_0, g_\beta)\}$ 
26:         end for
27:       end for
28:     end for
29:   return  $\mathcal{F}$ 
30: end function

```

1) *Cross Layer Connectivity (CLC)*: So far we have no way to estimate the impact of the resulting split configurations on the network performance. Previous work showed that connections across groups can have a positive impact on accuracy [26]. In the following we want to quantify that connectivity. We denote the total number of input channels in layer α that can influence a single output channel of layer β by c^* and the total number of groups from layer α , that are

processed by each individual filter kernel of layer β by n . It is obvious that $c^* = n \cdot s_{\alpha, \text{in}}$. The value n depends on the output size $s_{\alpha, \text{out}}$ and input size $s_{\beta, \text{in}}$, it determines how many of the g_α groups will influence the result of each of the g_β groups.

$$n = \left\lceil \frac{s_{\beta, \text{in}}}{s_{\alpha, \text{out}}} \right\rceil = \left\lceil \frac{f_\alpha \cdot g_\alpha}{g_\beta \cdot f_\alpha} \right\rceil = \left\lceil \frac{g_\alpha}{g_\beta} \right\rceil \quad (16)$$

We express the CLC of a Split Convolutional Block (F_α, F_β) as the fraction of input channels c_α that can impact each of the output channels f_β .

$$\text{CLC}(F_\alpha, F_\beta) = \frac{c^*}{c_\alpha} = n \frac{s_{\alpha, \text{in}}}{c_\alpha} = \frac{1}{g_\alpha} \cdot \left\lceil \frac{g_\alpha}{g_\beta} \right\rceil \quad (17)$$

As an example consider the split convolution visualized in Figure 4. Using $c_\alpha = 6, g_\alpha = 3, f_\alpha = c_\beta = 6, g_\beta = 2$, we obtain $\text{CLC}(F_\alpha, F_\beta) = \left\lceil \frac{3}{2} \right\rceil \cdot \frac{1}{3} = \frac{2}{3}$. Four out of six input channels c_α will influence the result of each output channel. A CLC of $\frac{2}{3}$ means that the Split Convolutional Block realizes

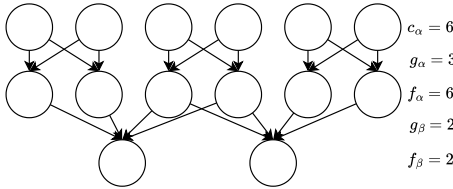


Fig. 4: Exemplary visualization of a split convolution with a CLC of $\frac{2}{3}$. Nodes represent an input or output channel.

two completely separate data paths, while $\frac{2}{3}$ means that there is an overlap where some input groups impact the result of more than one output group.

2) *Split Configuration Choice*: The intuition is that high fan in and high CLC should provide higher network performance. At the same time, we only want to consider configurations with high LUT-cost if their increased cost results in better performance. Our proposed score \mathcal{S} for split configurations is

$$\mathcal{S}(F_\alpha, F_\beta) = \frac{\text{CLC}(F_\alpha, F_\beta)^2 \cdot \phi_\alpha \cdot \phi_\beta}{\log(C(\phi_\alpha) + C(\phi_\beta))^2}, \quad (18)$$

where $F_{\alpha, \beta}$ denote the parameter tuples of the first and second convolution and $\phi_{\alpha, \beta}$ their fan ins.

We propose to find a network topology by choosing the top scoring configurations with a cost, that fits the use case, train them and select the architecture with best fit.

F. Toolchain and Hardware Implementation

We implement the approach as an extension of our elastic-AI creator tool¹. It automatically identifies precomputable blocks by their enclosing binary activations using pattern matching on an intermediate representation (IR). Then it replaces them in the IR with precomputed blocks by computing the corresponding truth tables. The right side of Figure 3 shows three such blocks in the post-training phase and their resulting precomputed counterparts.

¹open source available at <https://github.com/es-ude/elasticai.creator.git>

Finally, the tool converts the IR to a fully pipelined RTL-level VHDL specification of the model. The resulting implementation can then be verified with a previously stored data set, e.g., a subset of the training data, via simulation. Furthermore, the implementation does not use proprietary libraries or language constructs and is therefore portable to FPGAs from other manufacturers.

IV. EXPERIMENTS

This section describes the data set, training of proposed model architecture, their results and hardware utilization.

A. Dataset Handling and Training Properties

We evaluate the performance of the split convolutions on the MIT-BIH atrial fibrillation dataset [15] with the binary classification problem of detecting atrial fibrillation in ECG recordings. The dataset contains 25 long-term ECG recordings, each with a duration of 10 hours and two channels. The recordings have a resolution of 12 bits. We subsample the records by selecting every second data point, resulting in a sampling rate of 125 Hz. We partition 16 records into windows of about 42 s, resulting in about 13,800 examples, labelled as atrial fibrillation or sinus rhythm. The first channel turned out to be sufficient for the problem, so we ignore the second channel. For each split configuration, we perform an experiment consisting of six training runs over 400 epochs with a batch size of 1,024. We use binary cross entropy loss, the Adam optimizer with a learning rate of $5e^{-3}$ and decay the learning rate by 0.5 every 50 epochs. One run takes about 13 minutes using an NVIDIA RTX 8000 GPUs.

B. Model architecture and results

Table I shows the architecture of the model based on previous work [13]. Except for the first Split Convolutional Block, we use the same split configuration over the whole network, selected using Algorithm 1. To see the impact of the

TABLE I: Network Architecture for MIT-BIH data set. c_0 denotes the number of input channels chosen. Experiments have been performed for c_0 ranging from 6 to 12.

Layer	kernel size	in channels	out channels	stride
conv1d	1	1	12	1
bnorm	-	-	-	-
binarize	-	-	-	-
SplitConv	10	12	c_0	1
maxpool1d	8	-	-	6
SplitConv	6	c_0	c_0	1
maxpool1d	3	-	-	2
SplitConv	6	c_0	c_0	1
maxpool1d	3	-	-	2
SplitConv	6	c_0	c_0	1
maxpool1d	3	-	-	2
linear	1	c_0	1	-
sigmoid	-	-	-	-

reordering step described in Section III-D, we use this model architecture with 10 channels and train the two variants, (i)

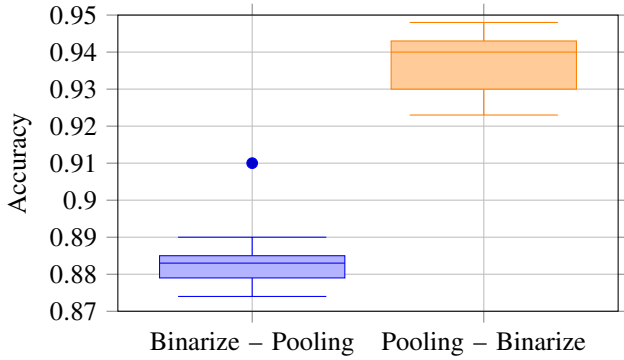


Fig. 5: Accuracy for different pooling positions for training.

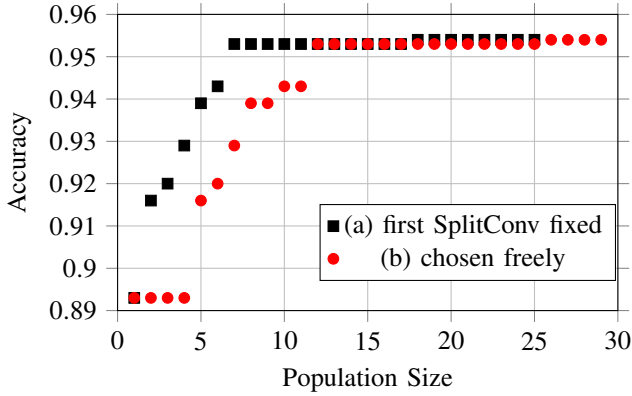


Fig. 6: Accuracy of the best model in the population for increasing population sizes.

max pooling layer between batch norm and convolution, (ii) max pooling layer after binarization. Figure 5 shows that the order has a significant impact. The version with the pooling after binarization has a lower accuracy by 5%.

Next, we want to understand the impact of our choice to always end Split Convolutional Blocks with a point-wise convolution (see Section III-C). The order of kernel sizes in a Split Convolutional Block has only little influence on the cost. Therefore, we study the resulting accuracy of both variants. The mean and standard deviation of accuracy achieved by the two kernel orders are $83.27 \pm 0.9\%$ for $(k_0, 1)$ and $81.05 \pm 0.7\%$ for $(1, k_0)$. This indicates that kernel size order $(k_0, 1)$ achieves better accuracy. This confirms our design choice.

Next, we want to find out how suitable our score is to find good split configurations. For the first experiments, we keep the configuration for the first Split Convolutional Block fixed to correspond to a depthwise separable convolution and only change the configurations for the other blocks. This results in 73 possible split configurations. To estimate the effort of finding a configuration with good accuracy that still fits on small FPGAs with 8k LUTs. We sort these configurations by their score, choose an increasing population of the first n configurations (varied from 1 to 30), train them, and select the model with the best accuracy. The result is visualized with case (a) in Figure 6. The approach reaches a plateau after increasing the population size to seven.

Typically, one needs to find configurations for many different layers, that are varied independently of each other. Thus, we repeat the same experiment but also vary the configuration for the first Split Convolutional Block. To set a score for the whole network, we compute the mean over the scores of all layers. Increasing the population size again, we find the result visualized with case (b) in Figure 6. Due to the filtering for analytic LUT-costs below 8,000, this results in 115 possible split configurations. With this setup, the approach reaches the plateau for a population size of twelve. The plateau is reached in both cases after increasing the population size to contain about 10% of the full configuration set resulting in a drastic search space reduction.

Next, we evaluate how well the score captures the intuition of rewarding models for a good trade-off between cost and accuracy in comparison to other candidates. We can formalize the intuition as follows: Let i, j be any two of these split configurations, A_i, A_j their corresponding accuracy, S_i, S_j their score and C_i, C_j their analytic cost, then we should always find

$$S_i < S_j \Rightarrow (A_i < A_j) \vee (C_i > C_j) \quad (19)$$

Again, we keep the first Split Convolutional Block fixed with a configuration that corresponds to a depth-wise separable convolution and only vary the other blocks. We choose a channel size of twelve, as this allows for more split configurations than values between six and eleven. We generate split configurations using Algorithm 1 with a maximum fan in $\phi_{\max} = 12$. Removing all configurations that would increase the LUT-cost to more than 8,000 leaves 24 possible choices for the other blocks. For the 24 remaining choices we find that 275 out of 276 pairs fulfil Equation (19). The single outlier pair can be found in the last row of Table II. Both configurations have a very small score, high cost and low accuracy compared to pareto-optimal configurations: Thus, both models would not be considered for training in a practical scenario.

When allowing the number of input channels for each channel to be chosen freely, we obtain 73 possible choices, resulting in 2,628 pairs. Table II lists all pairs that violate Equation (19). Only two of these pairs show an accuracy above 90% with a difference of 1%. Next, we want to find out how many of the best architectures wrt. the score must be trained to find the models that make up the pareto front. Ideally, the supremum of these architectures would correspond to that front. Table III shows this pareto front. The first thing to note is that one of the eleven configurations also appears in Table II as it violates the score condition. The configuration $(12, 6, 12, 24, 1, 3, 12)$ in the fifth row of Table III is part of the pareto front and outperforms two other configurations with higher score. While the accuracy of the configuration on the first row of Table III is only slightly better than that of the configuration below with higher score, looking at the value for f_α indicates that the score underestimates this value's impact. To cover the full pareto front it is sufficient to apply a threshold of > 5.0 to the set of configurations.

TABLE II: Pairs that violate (19). The first Split Convolutional Block is fixed to correspond to a depthwise separable configuration.

	Split Config.	Score	LUTs	Acc.	F1
<i>j</i>	(10, 6, 10, 10, 1, 1, 10)	20.62	3,087	93.86	93.31
<i>i</i>	(12, 6, 12, 24, 1, 3, 12)	6.52	2,713	93.92	93.41
<i>j</i>	(10, 6, 10, 20, 1, 2, 10)	10.14	3,127	93.03	92.49
<i>i</i>	(12, 6, 12, 24, 1, 3, 12)	6.52	2,713	93.92	93.41
<i>j</i>	(6, 6, 6, 24, 1, 6, 6)	1.07	2,059	75.61	75.09
<i>i</i>	(6, 6, 6, 18, 1, 6, 6)	0.70	2,011	76.51	75.08
<i>j</i>	(8, 6, 8, 32, 1, 8, 8)	0.69	2,293	76.10	75.17
<i>i</i>	(7, 6, 7, 21, 1, 7, 7)	0.55	2,120	76.38	75.01
<i>j</i>	(8, 6, 8, 8, 1, 4, 8)	0.59	2,133	74.35	72.11
<i>i</i>	(7, 6, 7, 21, 1, 7, 7)	0.55	2,120	76.38	75.01
<i>j</i>	(8, 6, 8, 32, 1, 8, 8)	0.69	2,293	76.10	75.17
<i>i</i>	(8, 6, 8, 24, 1, 8, 8)	0.45	2,229	76.60	74.92
<i>j</i>	(10, 6, 10, 10, 1, 5, 10)	0.41	2,327	74.65	74.19
<i>i</i>	(8, 6, 8, 16, 1, 8, 8)	0.25	2,165	74.79	72.27
<i>j</i>	(12, 6, 6, 12, 1, 12, 12)	0.08	6,505	73.21	71.16
<i>i</i>	(12, 6, 6, 6, 1, 6, 12)	0.05	4,465	75.50	72.89

TABLE III: Pareto front of split configurations with depthwise separable first Split Convolutional Block.

Split Configuration ($c_\alpha, k_\alpha, g_\alpha, f_\alpha, k_\beta, g_\beta, f_\beta$)	Score	LUTs	Acc.	F1
(12, 6, 12, 36, 1, 3, 12)	5.94	6,601	95.37	94.95
(12, 6, 12, 12, 1, 1, 12)	17.94	6,505	95.34	94.94
(12, 6, 6, 6, 1, 1, 12)	11.03	4,465	94.40	93.93
(11, 6, 11, 11, 1, 1, 11)	19.00	4,228	94.31	93.83
(12, 6, 12, 24, 1, 3, 12)	6.52	2,713	93.92	92.29
(9, 6, 9, 9, 1, 1, 9)	22.17	2,554	92.93	92.30
(8, 6, 8, 16, 1, 2, 8)	11.85	2,261	92.40	91.81
(8, 6, 8, 8, 1, 1, 8)	25.62	2,229	92.05	91.41
(7, 6, 7, 7, 1, 1, 7)	26.48	2,064	91.63	91.10
(6, 6, 6, 12, 1, 2, 6)	12.93	1,939	89.51	88.49
(6, 6, 6, 6, 1, 1, 6)	34.98	1,915	89.30	88.47

This would select 19 out of 73 possible configurations. Put differently, training 26% of the best configurations wrt. the score is sufficient to cover the pareto front in this experiment.

C. Hardware Utilization

All hardware accelerators are synthesized with AMD Vivado 2023.1 and deployed on the AMD Spartan-7 S15 FPGA.

In addition to the neural network, the accelerator also features a BRAM input buffer to store an entire data sample and logic that allows control via an SPI interface. The required clock cycles are mainly dictated by the size of the data sample, as data is processed in a sequentially to save area. The system takes one clock cycle per time step of the data sample. To avoid measuring the SPI communication between MCU and FPGA, we modify the hardware implementation to perform thousand inferences instead of one before signalling done. For an atrial fibrillation model with depthwise-separable styled split convolutions, we measure the time starting between signalling start of computation until the accelerator signals done. We measure 50.88 μ s per inference at a clock period of 10ns, i.e., approximately 5,088 clock cycles per inference, close to the 5,085 clock cycles we read from simulation. We can successfully generate the design for clock rates of up to 143 MHz.

By the nature of our approach, none of the synthesized designs consumes any DSP slices. The previous analytic cost estimations only consider the implementation of the neural network and ignore any of the logic required to interact with the MCU or manage the BRAM input and output buffers. For all our synthesized designs Vivado estimates a total power consumption between 42 mW and 65 mW with 20 mW of static power consumption. The numbers show a weak negative correlation of -0.4 between analytic LUT cost and power consumption. The power consumption estimated for the network component directly correlates with the networks size and ranges from 2 mW (network with 200 LUTs) to 5 mW (networks with 8k LUTs). As the reported post optimization LUT costs include additional components, the actual LUT consumption for very small networks with less than 600 analytic LUTs tends to be almost doubled. As networks grow larger the static overhead from other logic plays a smaller role and the use of dedicated muxing primitives and other logic optimizations become more important. As a result, bigger models (for which we analytically estimate three to 6k LUTs) need only half as many LUTs.

D. Comparison to related work

Finally, we compare our performance with related work on atrial fibrillation on FPGAs. Table IV summarizes the hardware utilization (LUTs, DSP slices, FFs) and the network performance (accuracy, F1, latency) for different model architectures. All examples are detecting atrial fibrillation using the MIT-BIH database. We compare with two of our selected configurations. BIG is the best selected model that still fits on our target platform. It has (12, 10, 12, 12, 1, 1, 12) for its first Split Convolutional Block and (12, 6, 12, 12, 1, 1, 12) for all others. SMALL for comparison is our best tiny network with (12, 10, 12, 12, 12, 2, 10) for its first Split Convolution and (10, 6, 10, 10, 1, 2, 10) for its other blocks.

TABLE IV: Comparison to other atrial fibrillation detectors using different model architectures on hardware

Approach	LUTs	DSP	FF	Accuracy / F1	Latency [μ s]
ViT [27] ^{χ}	53,810	131	24,026	99.0 / 99.4	3,830
1D Incept. [28] ^{χ}	26,987	448	-	99.3 / 99.0	231
1D Incept. [29] ^{χ}	28,758	80	13,313	99.5 / 99.2	22
2D-CNN [30] ^{χ, β}	20,198	98	12,993	91.9 / -	-
1D-CNN [31] ^{χ}	8,752	77	5,303	96.4 / 93.5	66
1D-CNN [32] ^{γ}	3,802	5	1,848	- / 95.8	-
arrWNN [33] ^{α, ρ}	-	0	-	88.2 / 81.3	-
BIG (ours) ^{χ, ρ}	2,844	0	871	95.8 / 95.6	51
1D-CNN [13] ^{χ, ρ}	2,352	0	-	94.2 / -	52
1D-CNN [13] ^{χ, ρ}	986	0	-	82.4 / -	52
SMALL (ours) ^{χ, ρ}	536	0	785	88.4 / 87.4	51

α : custom IC, γ : Lattice iCE40UP5K, χ : AMD FPGAs
 β : four labels, ρ : precomputed, -: not specified

The results show that our models achieve competitive performance with very tight hardware constraints. SMALL has the smallest footprint and acceptable performance. BIG performs comparable to [32] with a far smaller footprint.

The Vision Transformer ViT [27] and the 1D-CNNs with inception blocks achieve the highest accuracy and F1-score, but all of them drastically exceed out target platform's resources. The 2D-CNN is even outperformed by the non-precomputed 1D-CNNs wrt. resource requirements and performance. The only non LUT-based approach suitable for our hard resource constraints is the implementation of a 1D-CNN found through HW-aware NAS by Loroch et al. [32], using a Lattice instead of an AMD FPGA. The last five rows show LUT-based approaches. The arrWNN [33] uses a custom IC instead of an FPGA. Their resource utilization cannot be compared directly.

V. CONCLUSION

We reduce the fan-in of a 1D convolutional neural network to make LUT-based precomputation for ultra-low resource FPGAs feasible. This enables the realization of smart embedded sensor systems that use local machine learning to process sensor data. We defined a score based on fan in, LUT-costs and layer connectivity that allows us to estimate the models' trade-off between performance and costs. With this we show how to reduce the search space of possible architectures while staying pareto optimal. We obtain very efficient accelerators with good performance compared to related work. In future work, we want to evaluate our approach on additional time-series datasets, e.g., the CHB-MIT database for seizure prediction [34], to further study generalizability. Additionally, we want to explore combining our approach with others such as NeuralUT [35] or logic gate networks [20].

REFERENCES

- [1] O. Avci, O. Abdeljaber, S. Kiranyaz, and D. Inman, "Structural damage detection in real time: implementation of 1D convolutional neural networks for SHM applications," in *IMAC*, 2017, pp. 49–54.
- [2] T. Ince, S. Kiranyaz, L. Eren, M. Askar, and M. Gabbouj, "Real-time motor fault detection by 1-D convolutional neural networks," *IEEE Trans. Ind. Electron.*, vol. 63, no. 11, pp. 7067–7075, 2016.
- [3] L. Eren, T. Ince, and S. Kiranyaz, "A generic intelligent bearing fault diagnosis system using compact adaptive 1D CNN classifier," *Jour. Sig. Pro. sys.*, vol. 91, no. 2, pp. 179–189, 2019.
- [4] S. Kiranyaz, T. Ince, and M. Gabbouj, "Real-time patient-specific ECG classification by 1-D convolutional neural networks," *IEEE Trans. Biom. Eng.*, vol. 63, no. 3, pp. 664–675, 2015.
- [5] D. Li, J. Zhang, Q. Zhang, and X. Wei, "Classification of ECG signals based on 1D convolution neural network," in *IEEE Healthcom*, 2017, pp. 1–6.
- [6] F. Mattioli, C. Porcaro, and G. Baldassarre, "A 1D CNN for high accuracy classification and transfer learning in motor imagery EEG-based brain-computer interface," *J. Neu. Eng.*, vol. 18, no. 6, 2022.
- [7] P. Löhler, A. Albert, L. Heyermann, G. Schiele, K. Seidl, and A. Erbslöh, "Classification of ON- and OFF-Retinal Ganglion Cell Types in Extracellular Recordings," in *Proc. Workshop Biosignal*, 2024.
- [8] T. Ling, C. Qian, P. Zdankin, T. Weis, and G. Schiele, "StrikeWatch: Wrist-worn Gait Recognition with Compact Time-series Models on Low-power FPGAs," in *IEEE AIoT*, 2025.
- [9] S. Mittal, "A survey of FPGA-based accelerators for convolutional neural networks," *Neu. comp. and appl.*, vol. 32, no. 4, 2020.
- [10] Y. Umuroglu, Y. Akhauri, N. J. Fraser, and M. Blott, "LogicNets: Co-Designed Neural Networks and Circuits for Extreme-Throughput Applications," *arXiv:2004.03021*, Apr. 2020.
- [11] M. Andronic and G. A. Constantinides, "PolyLUT: learning piecewise polynomials for ultra-low latency FPGA LUT-based inference," in *IEEE ICFPT*, 2023, pp. 60–68.
- [12] M. Nazemi, A. Fayyazi, A. Esmaili, A. Khare, S. N. Shahsavani, and M. Pedram, "NullaNet Tiny: Ultra-low-latency DNN Inference Through Fixed-function Combinational Logic," *arXiv:2104.05421*, Apr. 2021.
- [13] L. Einhaus, C. Qian, C. Ringhofer, and G. Schiele, "Towards Pre-computed 1D-Convolutional Layers for Embedded FPGAs," in *ECML PKDD*, 2021, pp. 327–338.
- [14] G. H. A. Krizhevsky, I. Sutskever, "ImageNet Classification with Deep Convolutional Neural Networks," in *NeurIPS*, 2012.
- [15] G. Moody, "A new method for detecting atrial fibrillation using RR intervals," *Proc. Comput. Cardiol.*, vol. 10, pp. 227–230, 1983.
- [16] M. Andronic and G. A. Constantinides, "NeuraLUT: Hiding neural network density in boolean synthesizable functions," in *IEEE FPL*, 2024, pp. 140–148.
- [17] A. Khataei and K. Bazargan, "CompressedLUT: An Open Source Tool for Lossless Compression of Lookup Tables for Function Evaluation and Beyond," in *ACM/SIGDA Int. Symp. on FPGAs*, 2024, p. 2–11.
- [18] A. Ebrahimi, V. N. Pullu, J. Pierre Langlois, and J.-P. David, "Iterative Pruning Algorithm for Efficient Look-up Table Implementation of Binary Neural Networks," in *IEEE NEWCAS*, 2023, pp. 1–5.
- [19] O. Cassidy, M. Andronic, S. Coward, and G. A. Constantinides, "ReducedLUT: Table Decomposition with "Don't Care" Conditions," in *Proc. ACM/SIGDA Int. Symp. on FPGAs*, 2025, p. 36–42.
- [20] F. Petersen, C. Borgelt, H. Kuehne, and O. Deussen, "Deep Differentiable Logic Gate Networks," in *NeurIPS*, vol. 35, 2022, pp. 2006–2018.
- [21] F. Petersen, H. Kuehne, C. Borgelt, J. Welzel, and S. Ermon, "Convolutional Differentiable Logic Gate Networks," in *NeurIPS*, vol. 37, 2024, pp. 121 185–121 203.
- [22] I. Aleksander, M. De Gregorio, F. Franca, P. Lima, and M. H., "A brief introduction to Weightless Neural Systems," in *ESANN*, 2009.
- [23] S. Nag, A. T. Bacellar, Z. Susskind, A. Jha, L. Liberty, A. Sivakumar, E. B. John, K. Kailas, P. M. Lima, N. J. Yadwadkar, F. M. França, and L. K. John, "LL-ViT: Edge Deployable Vision Transformers with Look Up Table Neurons," in *IEEE ICFPT*, 2025, p. 19–29.
- [24] I. Hubara, M. Courbariaux, D. Soudry, R. El-Yaniv, and Y. Bengio, "Binarized Neural Networks: Training Deep Neural Networks with Weights and Activations Constrained to +1 or -1," *NeurIPS*, Feb. 2016.
- [25] M. Rastegari, V. Ordonez, J. Redmon, and A. Farhadi, "XNOR-net: Imagenet classification using binary convolutional neural networks," in *Lecture Notes in Computer Science*, vol. 9908 LNCS, 2016.
- [26] X. Zhang, X. Zhou, M. Lin, and J. Sun, "Shufflenet: An extremely efficient convolutional neural network for mobile devices," in *IEEE CVPR*, 2018, pp. 6848–6856.
- [27] S. Chandrasekaran, S. Chandran, and I. J. Selvam, "FPGA-Based Implementation of Real-Time Cardiologist-Level Arrhythmia Detection and Classification in Electrocardiograms Using Novel Deep Learning," *J. Circuit Theory and Applications*, vol. 53, no. 6, pp. 3662–3683, 2025.
- [28] N. L. N. Nhat and T. D. Tran, "Efficient ECG Beat Classification Using Inception Network on Software and FPGA Platforms," in *IEEE ICDV*, 2025, pp. 67–72.
- [29] H. L. Pham, T. D. Tran, V. T. D. Le, T. H. Vu, and Y. Nakashima, "A Fast and Memory-Efficient CNN Accelerator for ECG Classification in Remote Healthcare Systems," in *Int. Conf. ECTI-CON*, 2025, pp. 1–6.
- [30] L. Greco, F. Moscato, P. Ritrovato, and M. Vento, "Fast and low cost FPGA-based architecture for arrhythmia detection with CNN," *Internet of Things*, vol. 33, p. 101705, 2025.
- [31] H. Tianyi, J. Yuchen, W. Yijing, L. Qinghui, and L. Dakun, "Deep Learning Based Automatic Detection Algorithm of Atrial Fibrillation Implemented on FPGA," in *IEEE PRML*, 2024, pp. 330–334.
- [32] D. Loroch, J. Feldmann, V. Rybalkin, and N. Wehn, "Low-power, Energy-efficient, Cardiologist-level Atrial Fibrillation Detection for Wearable Devices," in *IEEE SOCC*, 2025, pp. 1–6.
- [33] V. Pillai, I. D. S. Miranda, T. Musale, M. Jadhao, P. C. R. Souza Neto, Z. Susskind, A. T. L. Bacellar, M. Lhostis, P. M. V. Lima, D. L. C. Dutra, E. B. John, M. Breternitz, F. M. G. França, E. Ozer, and L. K. John, "arrWNN: Arrhythmia-Detecting Weightless Neural Network FlexIC," in *IEEE IFETC*, 2024, pp. 1–4.
- [34] J. Guttg, "CHB-MIT Scalp EEG Database (version 1.0.0)," 2010. [Online]. Available: <https://physionet.org/content/chbmit/1.0.0/>
- [35] M. Andronic and G. A. Constantinides, "NeuraLUT-Assemble: Hardware-aware Assembling of Sub-Neural Networks for Efficient LUT Inference," in *IEEE FCCM*, 2025, pp. 208–216.